11th Asia-Pacific Conference on Combustion,
The University of Sydney, NSW Australia
10th -14th December 2017.

SAND2017-13068C

Advanced optical diagnostics at engine conditions

Lyle M. Pickett[1]

[1]Sandia National Laboratories

PO Box 969 MS9053, Livermore, CA, 94551, United States of America

Abstract

Internal combustion and gas turbine engines operate at high-pressure and high-temperature conditions where there is a particularly a strong need to improve the accuracy and predictive capability of CFD models used for engine design. However, optical diagnostics at these conditions are challenging. To develop more complete and quantitative datasets for engine spray combustion, our group led the establishment of the Engine Combustion Network (ECN) in 2009, defining specific target operating conditions and providing the same fuel injector series to groups of international participants. Since 2009, new diagnostics have been developed, boundary condition control has improved, experiments have been repeated at separate institutions to define and reduce uncertainties, and the combined, leveraged dataset is publicly available for CFD validation and development activities (https://ecn.sandia.gov/). This paper and plenary talk briefly review several of the diagnostic advancements from our laboratory and by other ECN participants, contributing to improved understanding and quantitative datasets for both diesel and gasoline sprays.

1 Introduction

In the quest to produce clean and efficient engines at a reasonable cost, engine designers increasingly rely upon CFD simulations to minimize expensive hardware fabrication and testing. Clearly, success in the design optimization is dependent upon the predictive capability of available CFD, yet truly quantitative validation experimental data showing that CFD is indeed accurate at conditions applicable to engine combustion remains quite scarce. A partial list of the barriers preventing acquisition of this type of data includes: harsh, high-temperature and high-pressure conditions, complicated flow and turbulence, two-phase mixing via fuel injection sprays, and chemical reactions involving thousands of molecular species.

The Engine Combustion Network (ECN) is an experimental and modeling organization seeking to overcome these barriers [1]. Through international collaboration at the same charge-gas conditions, and using the same fuel injector controlled to specified conditions, a more complete dataset is being developed. The ECN contains a growing internet data archive library (http://www.ca.sandia.gov/ECN/) with well-documented diesel and gasoline spray experiments. Experimentalists verify that they can meet the boundary condition for the charge-gas and injector by direct measurement, and then apply new diagnostics that build upon past measurements and understanding. For example, over 70 different measurements have been performed at the Spray A target conditions. Because of the extensive dataset, the target conditions and parametric variations about these conditions become a focus for CFD efforts. To date, over twenty institutions have contributed experimental data to the ECN, and likewise, over twenty institutions have submitted CFD simulation results. Simulation results and new experimental data are provided for workshop activities, where organizers collect, analyze, present, and make recommendations for future research [1].

In the following sections of this paper, several of the new diagnostics are reviewed, along with the new understanding and modeling advancements facilitated by the diagnostic.

2 Quantifying liquid-phase vaporization

Fuel injection sprays mix with the charge-gas and vaporize. Understanding the extent of liquid-phase penetration is essential for engine design, as impingement upon the piston or cylinder liner surfaces is generally problematic. The extent of liquid penetration varies significantly as charge-gas conditions vary—pressurizing and heating the charge-gas through compression promotes vaporization and limits liquid penetration upon injection. Mie-scatter imaging experiments have been performed over a range of pressures and temperatures to characterize the liquid penetration during a quasi-steady period of injection (e.g. [2]). But defining liquid penetration using Mie-scatter techniques has proven challenging, and ultimately has been unsuccessful for standardization [3]. One problem is that defining the diagnostic as the farthest penetration of even the smallest droplet is impractical, since the scatter would eventually be competitive with scatter from gas molecules. Instead, the largest liquid penetration dataset was defined based upon a threshold referenced to 3% of the maximum intensity upstream in the plume [2]; in other words, not an absolute-zero liquid concentration. Referencing to a maximum intensity in the plume also proves problematic because of dependencies upon the lighting and imaging setup. For example, six different Mie-scatter setups produced different results at Spray A conditions in the same facility at the same Spray A operating conditions [3].

A preferred method for standard, and quantitative, liquid length measurements appears to be backlit extinction imaging, because of the ability to reference extinction to the initial intensity, I_0. Indeed, the SAE standard on gasoline fuel spray characterization requires backlit imaging and processing based upon I_0 [4]. Of course, this type of standardization and measurement is easier for an open spray at atmospheric conditions, rather than confined in an engine or pressurized high-temperature chamber. Nevertheless, the ECN has pursued backlighting as the standard for liquid-penetration length quantification. The sections below explain these developments, which required many special considerations because of the harsh operating conditions. Several significant findings from the liquid visualization investigations are also reviewed.

Corresponding author e-mail address: LMPicke@sandia.gov

2.1 Advances in lighting and imaging

Development of diagnostics suitable for liquid-spray quantification have been influenced strongly by advances in high-speed lighting and imaging technology since the formation of the ECN. High-speed imaging at speeds approaching 100,000 frames per second has become almost a necessity to understand engine spray behavior. This type of imaging indicates timing for the actual start and end of injection, even for multiple closely spaced injections that are becoming common for the industry, and it quantifies liquid penetration during all timing of the injection event rather than only a quasi-steady period as in the past.

Advances in high-speed CMOS cameras need to be coupled by high-speed lighting sources that can produce higher quantities of light, and also deliver short-duration pulses to freeze the scene at each frame. Two different advancements are noted. First, pulse-burst lasers have been developed to produce a limited number of high-energy pulses. For example, researchers at Sandia assembled a laser that delivers 500 pulse-pairs at 100 kHz, with approximately 30 mJ per pulse [5]. Second, researchers at Sandia have also developed inexpensive drivers for LEDs that can produce light pulses as short as 10 ns at MHz rates [6].

An example setup using multiple high-speed cameras and lighting systems applied to a constant-volume spray chamber is shown in Fig. 1. These coupled camera/lighting technologies have been utilized for quantitative diagnostics, including liquid-spray diagnostics discussed in Section 2.

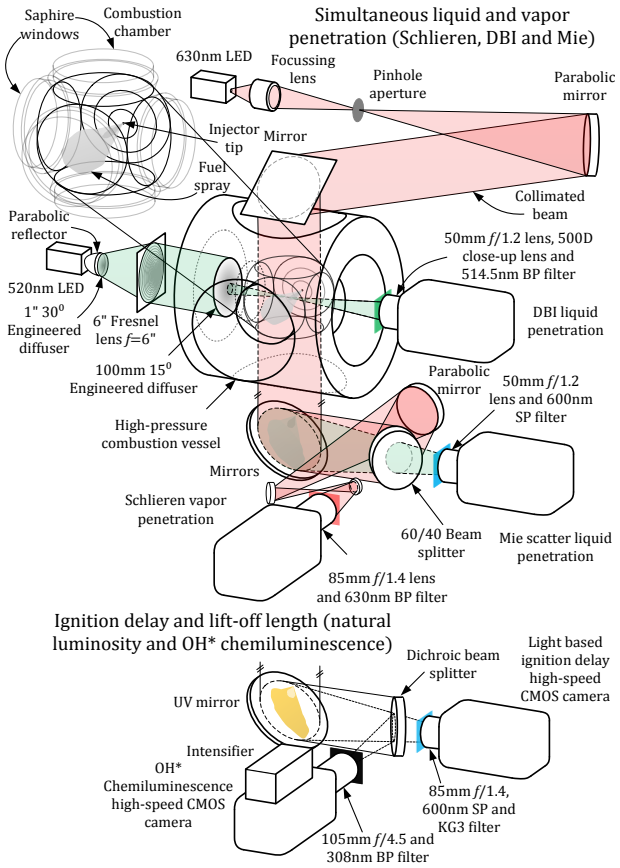

Figure 1: Spray chamber experimental setup featuring simultaneous high-speed imaging diagnostics. The lower section is for ignition/combustion imaging.

2.2 Overcoming beam-steering effects

A significant challenge that must be overcome to permit quantitative diagnostics in sprays at engine conditions is the optical distortion caused by beam steering from refractive index gradients. Figure 2 illustrates the problem. Schlieren imaging, with collimated backlighting, is shown during the premixed combustion and cool-down event. The propagating flame is clearly indicated, but after the flame passes, and pressure and temperature decrease to the target ambient conditions (6. MPa, 900 K) prepared for spray injection, significant distortion remains [7]. These distortions are primarily caused by steering from the thermal boundary layer created between the high-temperature, high-density gases and the colder vessel windows. Since fuel injection begins at the time indicated, any diagnostic of the spray must be resilient to these beam-steering effects from just the charge-gas gradients. In addition, even more intense refractive index gradients are created by cold fuel vaporization within the fuel jet, as well as heat-release and high-temperature combustion. Direct measurements of the steering in reacting diesel jets show a collimated laser expanded approximately 150 mrads [8].

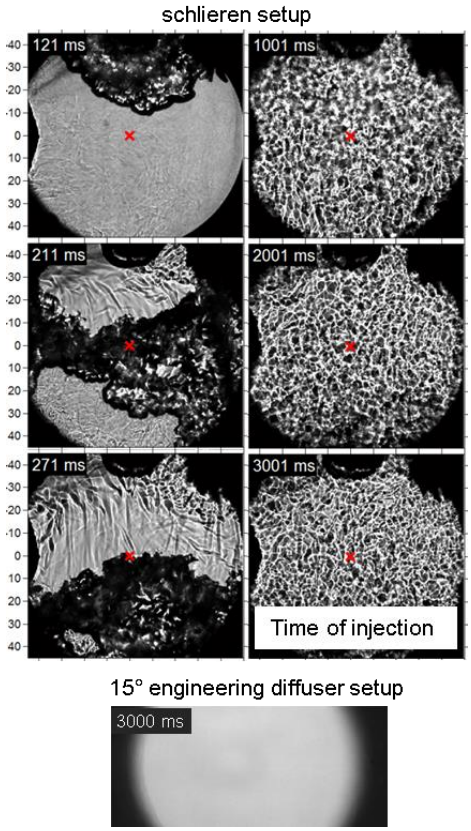

Figure 2: (top) Schlieren imaging during premixed combustion and cool-down in spray chamber. The timing of injection during the cool down determines the charge-gas temperature and pressure. (bottom) Backlighting with an engineering diffuser at the time of injection for 6 MPa, 900 K conditions.

To perform backlit imaging for quantitative liquid extinction, one can immediately conclude that schlieren backlighting, essentially designed to highlight refractive index gradients, will not be successful, which is confirmed by Ref. [7]. Diffused backlighting is another option. Indeed, the bottom of Fig. 2 shows that beam-steering disturbances are no longer detectible when backlit with diffused lighting. Beam steering still acts on individual rays, but the diffused ray bundle randomly distributes

on every camera pixel such that the effect is no longer apparent. Experience has shown, however, that backlighting from typical diffusers (e.g. ground glass or holographic), that appear to work perfectly fine at atmospheric conditions, is inadequate at engine conditions.

The theory as to why many typical diffuser lighting setups fail at these conditions is well documented in Ref. [6]. An improved diffused lighting arrangement, depicted as Diffused Backlit Imaging (DBI) in Fig. 1, is also discussed in detail in Ref. [6]. An essential feature for the setup is an equal (Lambertian) radiance that exceeds the level of jet beam-steering and overfills the collection angle of the receiving camera.

A demonstration for liquid extinction contrasting two different setups is shown for the Spray A conditions in Fig. 3. The optical thickness is shown over a tight display range near zero to highlight noise artifacts and to evaluate the potential for measurement when liquid has truly evaporated. The top image of measured optical thickness was taken with a setup that had insufficient diffused radiance angle, and it shows a noise artifact from cold fuel vapor that produces significant refractive index gradients. By contrast, the bottom image was obtained with sufficient diffused radiance angle, and the beam-steering artifacts from the fuel vapor are not present. Without the beam-steering artifacts, the actual liquid penetration is now quantified based upon metrics for extinction (optical thickness). The setup can be repeated in other facilities and at other operating conditions to quantify the liquid penetration with better consistency.

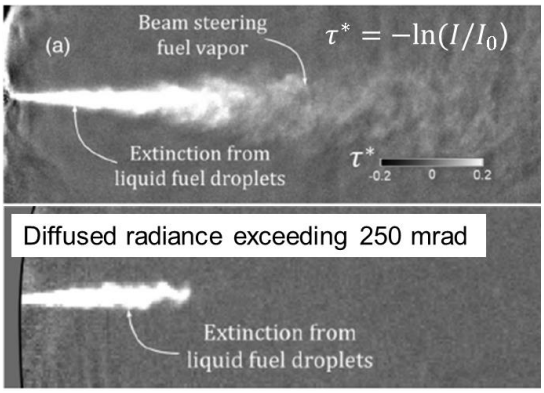

Figure 3: High-speed liquid extinction imaging at Spray A non-reacting (0% oxygen) conditions [1,6], displayed over range of optical thickness near zero. (top) Insufficient diffused radiance showing remnants of vapor-phase beam steering. (bottom) imaging setup with larger diffused radiance, and 150 kHz imaging.

2.3 Transcritical conditions

While it is known that the charge-gas conditions exceed the critical temperature of the fuel, a typical cooled liquid fuel injector delivers liquid in a subcritical state. Therefore, one cannot assume that the mixing processes for liquid fuel injection are supercritical, as if the system were single-component and the compressed liquid was above the critical temperature. Until recently, the optical difficulties highlighted above had impeded clear visualization of microscopic droplets at realistic, transcritical operating conditions. The combination of improved lighting setup, coupled to high-speed imaging, proved essential for studies of the liquid structure at conditions that may approach supercritical behavior. The optical setup included diffused backlighting, but a long-distance microscope lens was employed to provide measurements with high spatial and temporal resolution [10].

Figure 4 shows results of this imaging at three different charge-gas pressures and temperature, when injecting liquid n-dodecane at 373 K. The gas is inert (0% oxygen). A time period after the end of injection is selected because the velocity of the liquid slows such that it can be tracked within the same image. The top panel at 700-K conditions shows a shrinking sphere, as expected for classical vaporization with liquid surface tension. Visualization showed that the Spray A condition at 900 K and 6.0 MPa falls into this classification. The middle panel at 1000-K conditions shows a liquid sphere that at first exhibits surface tension and elastic behavior. But with time, sections of the liquid stop exhibiting surface tension. The bottom panel at 1200-K and 10.6 MPa conditions shows liquid structure that lacks surface tension, mixing in a diffusive fashion with the charge gas. However, even at these elevated pressure and temperature conditions, the transition to diffusive mixing does not occur instantaneously when the fuel enters the chamber. Rather, subcritical liquid structures exhibit surface tension in the near-nozzle region and then, after time surrounded by the hot ambient gas and fuel vapor, undergo a transition to a dense miscible fluid.

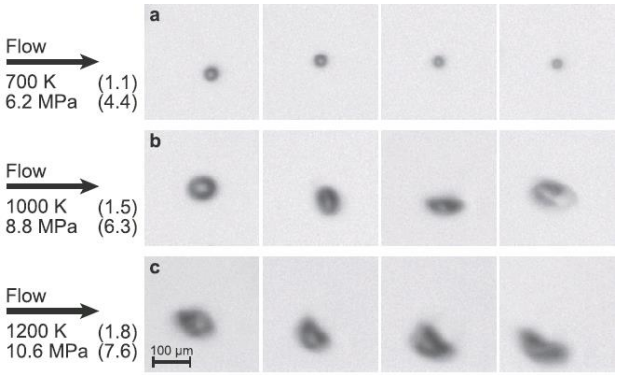

Figure 4: High-speed microscopic imaging of n-dodecane liquid structure at different charge-gas pressures and temperatures [10]. Dodecane fuel is injected at 373 K into the conditions indicated. A time sequence featuring isolated liquid structure produced after the end of injection is shown left to right.

This study demonstrates the remarkable finding that fuel injection at transcritical conditions, which is completely common for diesel injection, includes fuel sprays that may simultaneously exhibit regions with and without surface tension. This behavior must be addressed in CFD numerical models. Currently, most fuel injection models assume blobs or particles with surface tension, or a dense fluid without any surface tension (i.e. Navier-Stokes equations apply throughout), but nothing considering a transition from one regime to another. For reference, experiments using fuels wither higher and lower critical temperature are available [10]. Numerical models describing the theory of a time dependency for the transition to lack of surface tension at the interface have also been proposed [11].

2.4 Proximity of liquid to combustion

With improved ability to measure the liquid extent and structure at engine conditions, we can also address how the liquid structure may or may not affect combustion. For example, does diesel combustion occur with isolated burning droplets, or is the liquid phase not in close proximity to the flame?

Early visualization at the Spray A conditions shows that the latter

is the case. The measured axial liquid-penetration, even by various definitions, is less than 11 mm, while the ignition and lift-off length site is downstream of 17 mm [1]. Combustion occurs where mixtures of vaporized fuel mix with the charge-gas rather than with the liquid itself. However, since the Spray A nozzle is quite small (just 0.090 mm) and liquid penetration tends to scale with nozzle size [2], there is concern that the result would change if a larger, more-typical nozzle size were used.

Addressing this question, experiments have been conducted with a nozzle twice the diameter of Spray A. The Spray D nozzle diameter is 0.188 mm [12], and results from operation of Spray D at the same ambient and fuel injector conditions, using the optical setup shown in Fig. 1, are given in Fig. 5. The liquid length increases as expected, but the flame lift-off length also increases from 17 mm to 27 mm.

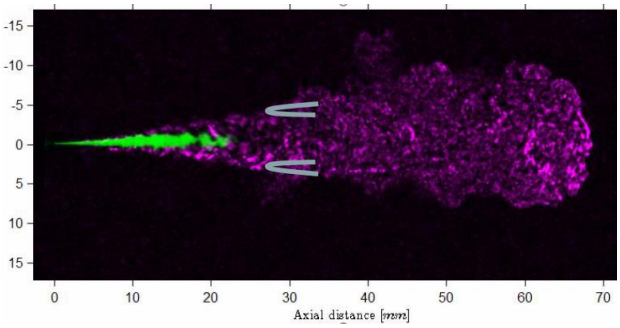

Figure 5: Overlay of liquid region from extinction imaging (green) and temporal difference of schlieren image (magenta) at non-reacting, 900 K, 6 MPa conditions. Added at 27 mm, is the expected location of the flame, based upon measurements at reacting (15% oxygen) conditions [12].

With improved capacity to definitively measure the liquid region as discussed above, and by combining this liquid region with vapor measurement from schlieren imaging, we observe that liquid is confined to the central region of the jet, while vapor extends towards the jet periphery. Model jet predictions at an axial distance of 27 mm show an equivalence ratio exceeding five at the centerline, and a near-stoichiometric zone at radial positions greater than 3 mm. At these high-temperature conditions, liquid appears to completely evaporate under fuel-rich conditions far from the flame. Even if liquid were to exist at the centerline (by increasing the nozzle size further), there is still no evidence that liquid would participates directly in the high-temperature flame, as the stoichiometric zones are at the periphery of the jet. The conclusion is that droplet/flame interactions may not exist whatsoever during the main period of diesel combustion. An exception could be the low velocity, dribble event at the end of injection. Gasoline spray combustion conditions are not considered by these statements.

In summary, advancements in diagnostics to quantify the liquid-phase penetration of diesel sprays have shown rapid and complete vaporization upstream of the flame. The overall behavior is consistent with mixing-dominant vaporization as proposed by Siebers [2], potentially assisted by a transition to diffusion mixing at transcritical conditions. However, truly quantitative measurements of mixture fraction are needed to assess if the spray mixes much like a momentum-driven gas jet, where droplets do not exist at all. Quantitative mixing measurements of the type needed for CFD validation are given in the next section.

3 Quantitative mixture fraction and velocity

3.1 Steady mixture fraction

Prior to the intensive effort of the ECN, no mixing data had been used to explore the validity of diesel spray mixing models, either with detailed CFD or with more simplistic analytical models for fuel jet mixing. Mixing measurements were performed using planar Rayleigh scattering [13]. By avoiding the liquid-phase portion of the spray, and after correction for laser intensity variation, the technique provides the mixture fraction, or fuel mass fraction, in the vapor region of the jet as shown in Fig 6.

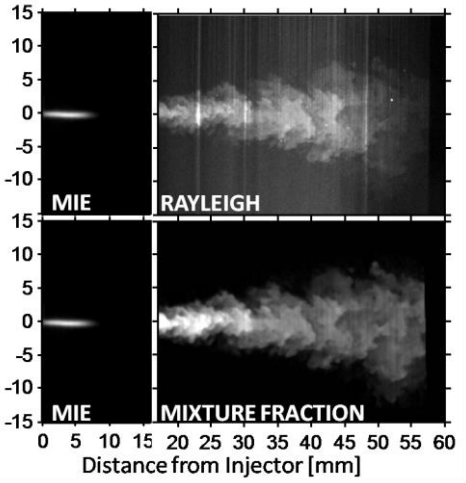

Figure 6: Composite image of Mie scattering (left) and Rayleigh scattering (right). Top is raw Rayleigh image with laser sheet propagating from the bottom. Bottom is corrected image for mixture fraction.

Mixture fraction data was obtained at the Spray A condition during the quasi-steady period of injection, after the head of the jet passed through the field of view. The average data are compared to predictions of the analytical jet model of Musculus and Kattke [14] in Fig. 7, where the 21.5° spreading angle setting also matched the measured jet penetration.

To illustrate how well the model compares to the experimental results in a meaningful, quantitative manner, we show the axial decay of centerline mixture fraction at the top and several radial profiles of mixture fraction at a particular axial position at the bottom. The ensemble-averaged experimental results are shown as blue lines, the model predictions as red lines, and measurement uncertainty 95% confidence intervals are shown as gray fill. If model predictions pass within the gray fill region, they are accurate within the uncertainty of the experimental measurements.

These results show that the radial distribution used in the Musculus and Kattke model, which resembles a Gaussian error function, is an appropriate representation of mixture fraction in a fully developed, vaporized diesel spray. The experimental (and model) mixture fraction for vaporized diesel sprays follows a self-similar distribution. The centerline mixture fraction decays inversely proportional to axial distance, and collapses when normalized by the jet outer radius. While these are well-known results for gas jets, the study at engine conditions is the first to convincingly demonstrate that vaporized diesel sprays are also self-similar.

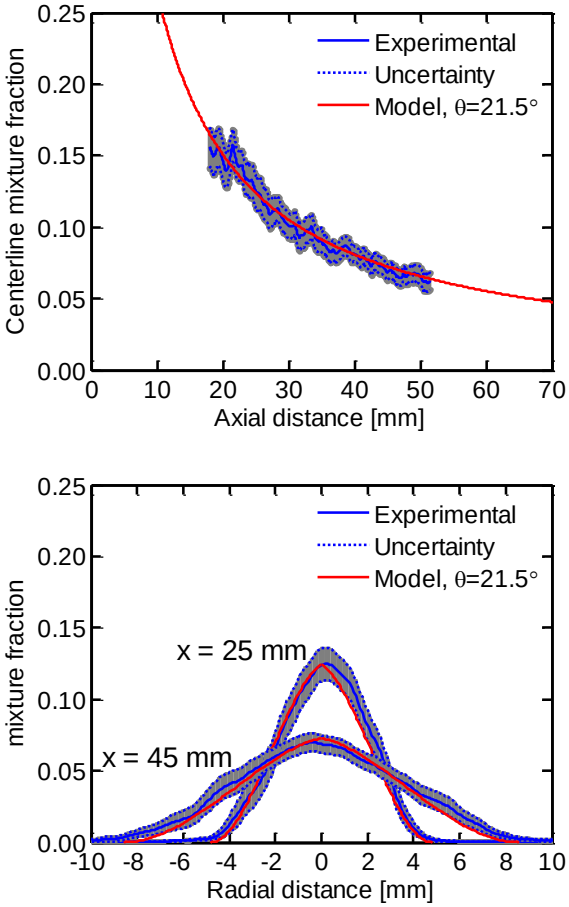

Figure 7: Measured mixture fraction and model predictions at centerline (top) and radial positions (bottom). Charge gas conditions: 900 K, 22.8 kg/m^3, 6.0 MPa. Injector conditions: 0.090-mm orifice, 150 MPa, n-dodecane, 363 K [13].

3.2 Velocity

Quantitative velocity measurements have also been performed in the vapor region of Spray A using high-speed PIV [15,16] at IFPEn and CMT-Motores Térmicos. Analysis shows that steady radial profiles are Gaussian and follow self-similarity scaling. In addition, mixing and velocity fields are consistent, i.e., a model that matches the mixing field also matches the velocity field, despite the fact that measurements were performed at different facilities using different Spray A injectors (but with the same specifications).

3.3 Transient mixture fraction

While valuable, and widely used as target data for CFD analysis, the above mixing and velocity results are limited to steady-state conditions. Understanding the transient mixing, and its impact on ignition and penetration, also requires special attention.

Recently, the aforementioned pulse-burst laser developed at Sandia was applied for planar Rayleigh scattering at 100 kHz rates, such that the mixing field is resolved for single injection events [17]. Similar to the Rayleigh setup described above, the liquid region was avoided to measure only vapor-phase mixing. Imaging was successful using a non-intensified high-speed CMOS camera, while performing corrections for background scatter and particle removal. Example processed mixture fraction images are shown at a few select timings in Fig. 8. The experiments provided two-dimensional mean and variance of the mixture and temperature quantities. The optical system's high spatial and temporal resolution enables tracking of the mixing field with time and space, from which temporally and spatially correlated mixing quantities can be extracted.

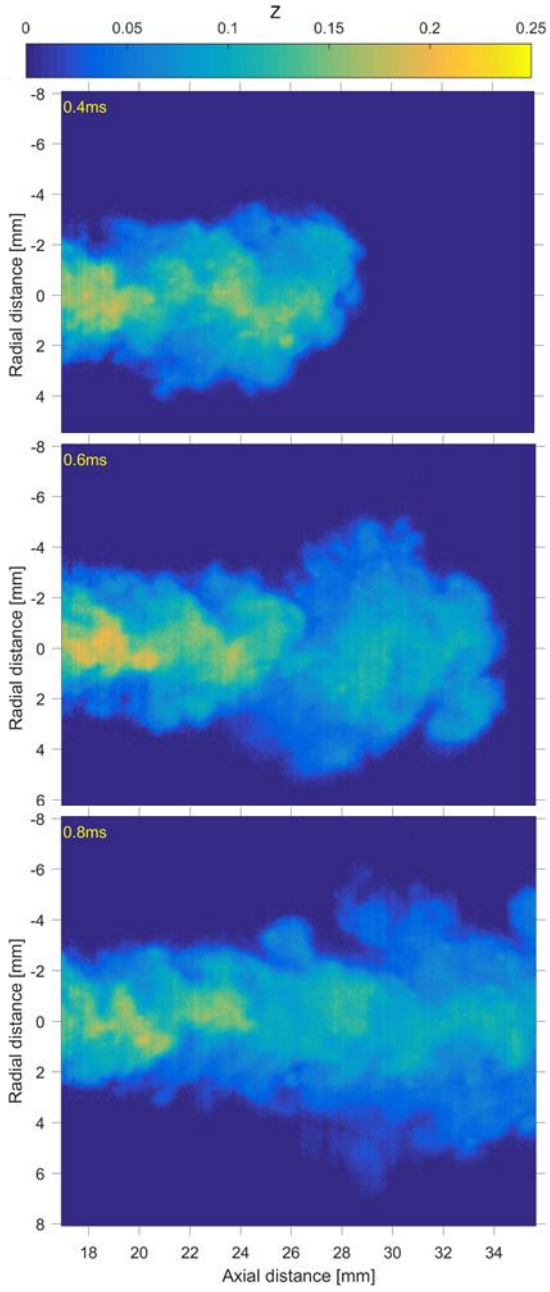

Figure 8: Select mixture fraction images for the non-reacting Spray A operating condition. Time after start of injection is given at the upper left [17].

In addition to the transient statistics, a major benefit of the pulse-burst system is the acquisition of enough data such that meaningful statistics can be computed with reduced uncertainty, and directly compared to CFD. Further analysis being pursued with this data includes classification of the ranges of scalar dissipation rates and turbulent length scales that can be resolved at the high-pressure (6 MPa) conditions.

4 Combustion

The importance of a solid dataset for liquid vaporization, mixing,

and velocity cannot be overstated, because of the direct effect of mixing on combustion behavior. In this final section, we now consider several advances in combustion diagnostics. Once again, the goal is quantification by metrics that can be directly compared to CFD simulations.

4.1 Cool-flame and high-temperature ignition imaging

Desiring to better understand the diesel ignition processes, a new high-speed diagnostic was once again applied at the ECN Spray A conditions. A simultaneous schlieren and formaldehyde (CH2O) planar laser-induced fluorescence (PLIF) imaging system was developed to investigate the low- and high-temperature auto-ignition events [18]. High-speed (150 kHz) schlieren imaging allowed visualization of the temporal progression of the fuel vapor penetration as well as the low- and high-temperature ignition events, while formaldehyde fluorescence was induced by a pulsed laser sheet at a select time during the same injection to provide information about the planar distribution of ignition.

As a diagnostic ultimately sensitive to temperature, research has shown that a "softening" of the schlieren effect begins prior to the onset of high-temperature ignition. To confirm that the softening of the schlieren effect is associated with low-temperature reactions, schlieren imaging was performed under both non-reacting and reacting conditions as shown in Fig. 9. The schlieren system was tuned for less sensitivity than that given in Fig. 2 by extending the light source size, and the image shown was also "tared" (corrected for the ambient disturbances) at the start of injection.

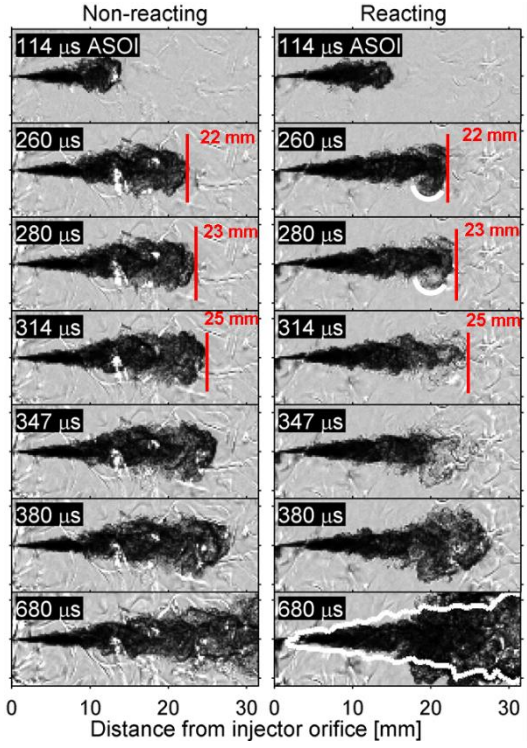

Figure 9: Time sequence of schlieren images resolving vapor penetration (for the non-reacting spray, left panels) and the low- and high-temperature ignition events (for the reacting spray, right panels). Spray A conditions.

The images at the left represent the schlieren of cold fuel vapor in refractive index contrast to the hot ambient without any reaction. Note that the appearance is similar to the reacting case at the right until approximately 300 µs ASOI, at which point the reacting case begins to show a "softening" effect near the head of the spray. More specifically, at the previous timing (260 µs ASOI), the lower portion of the "reacting" spray head is characterized by a dark semi-circular region. In the following frame (280 µs ASOI), this same structure is visible, however, the region appears lighter. This is a consequence of reduced gradients in the local refractive index, which result from a rise in the local temperature to values closer to the temperature of the ambient gases. This temperature rise can be attributed to heat release from the low-temperature auto-ignition reactions.

What may be surprising is that the "schlieren transparency" appears across the whole of the jet by 347 µs, which must indicate that the low-temperature reactions quickly move into the cool, fuel-rich section of the fuel jet. This activity is actually supported by modeling theory explaining how mixing with cool-flame products quickly propagates and accelerates the reaction into rich mixtures [19].

At later timings (380 µs), a schlieren boundary reappears indicating that high-temperature ignition has ensued, as confirmed by the associated pressure trace and high-speed chemiluminescence imaging under identical conditions. Now, the axial penetration boundary of the reactive species defined by the flame is consistent once again with the non-reacting vapor penetration. The bottom right panel at 680 µs shows that the quasi-steady lift-off length has been established in the reacting spray and can be identified by the abrupt radial expansion of the schlieren boundary near 17 mm. This radial expansion of the high-temperature products near the lift-off length has been emphasized by overlaying the non-reacting vapor boundary at this same timing as a white border.

The images in Fig. 10 represent a time sequence of paired formaldehyde PLIF and schlieren images, resolving the low- and high-temperature ignition events for the very same injection. False color images of the formaldehyde PLIF are presented in the left column. High-speed movies and LIF images acquired are also available on the ECN website [1]. The general conclusion from the analysis of the planar images in comparison to the schlieren at the same timing is that the schlieren imaging softening of refractive index gradients is indeed related to low-temperature heat release. Pockets of formaldehyde PLIF are found in the same regions indicated by the schlieren but the PLIF is more sensitive to the earliest appearance, highlighting the advantage of the planar technique. The transition to high-temperature ignition corresponds to a reappearance of the schlieren border at the edge of the jet and a decrease in formaldehyde in the same region. Overall, the experiments show that valuable information about low- and high-temperature ignition location and timing can be captured with the combined diagnostic, providing much-needed details for CFD model validation.

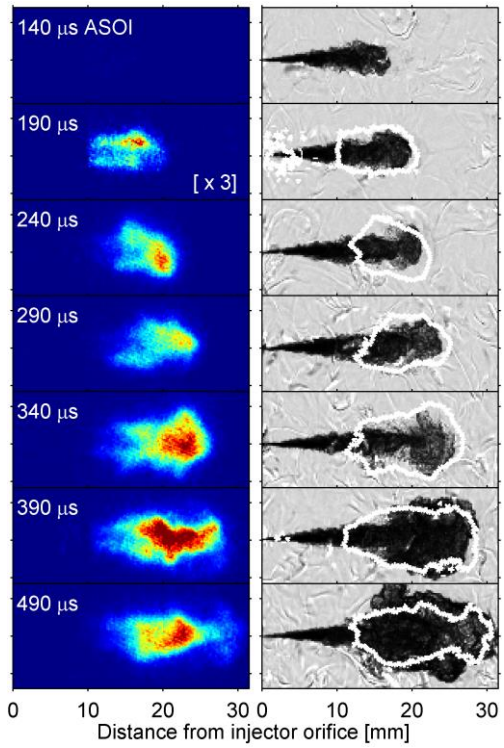

Figure 10: Time sequence of formaldehyde PLIF (left panels) and schlieren images (right panels) for Spray A.

4.2 Soot extinction imaging

The improvements in high-speed extinction imaging diagnostic, applied to measure liquid penetration above, are also beneficial for quantitative soot measurements. While there is uncertainty in the soot refractive index to relate an extinction measurement at a given wavelength to the soot volume along a line of sight, the soot particles are small and absorptive and offer less uncertainty for extinction compared to liquid droplets. Additional considerations include removal of the soot luminosity background, which can be accomplished by alternating dark and light frames between successive images much like a chopper wheel [20]

Figure 11 shows a comparison of soot optical thickness for two different style diesel fuel injectors. With cavitation and a larger spreading angle, Spray C generates a shorter lift-off length and an earlier position for soot formation compared to Spray D [12]. The spatial position and amount of soot formation can be quantitatively compared to CFD predictions. An open question is whether or not the total soot formation will be higher or lower for the cavitating fuel injector. With a wider spreading angle, one may expect more rapid mixing upstream. But the response to stabilize reactions closer to the injector may offset any positive effects of improved mixing. The ability to carefully understand and predict the spray, mixing, ignition, combustion stabilization are each necessary for successful prediction of soot formation and oxidation pathways.

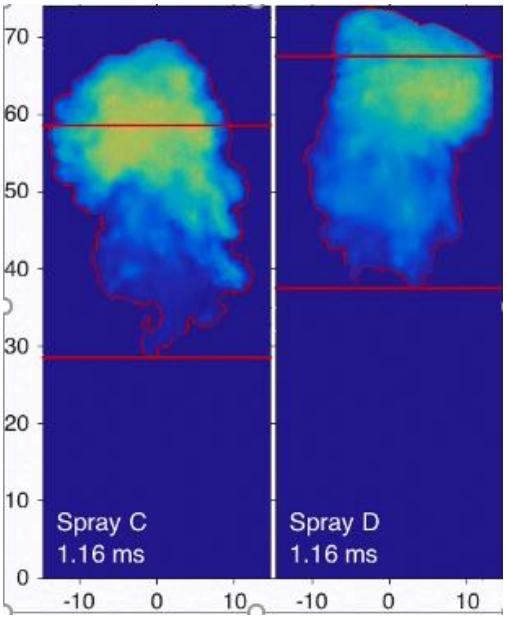

Figure 11: Soot optical thickness measured using high diffused radiance extinction imaging with a 623-nm LED source. Charge-gas conditions: 1000 K, 6.7 MPa, while other conditions are the same as Spray A.

5 Conclusions

The paper provides an overview of the diagnostic challenges that exist at engine conditions, and a summary of several advancements in diagnostics to meet these challenges. The progress of the Engine Combustion Network [1] to provide quantitative data sufficient to improve the predictive capability of CFD is discussed. New diagnostics are being developed to build upon a database of at least 60 different measurements that have already been performed at specific target operating conditions.

Relevant diesel spray conditions are highlighted throughout the paper, but there is also a parallel ECN activity in gasoline sprays with similar advancements in diagnostics capability.

These data are available online at https://ecn.sandia.gov/, with documentation having the express intent to provide all necessary information for CFD simulations, including geometries, boundary conditions, and uncertainties. Experimental and modeling participation using this data is encouraged.

6 Acknowledgment

I gratefully acknowledge the many experimental and modeling contributors to the ECN, and to the subject matter covered in this review.

The author is funded by the U.S. Department of Energy, Office of Vehicle Technologies, through program managers Gurpreet Singh and Leo Breton. Experiments were conducted at the Combustion Research Facility, Sandia National Laboratories, Livermore, CA. Sandia National Laboratories is a multi-mission laboratory managed and operated by National Technology and Engineering Solutions of Sandia, LLC., a wholly owned subsidiary of Honeywell International, Inc., for the U.S. Department of Energy's National Nuclear Security Administration under contract DE-NA0003525.

References

1. Engine Combustion Network data archive <https://ecn.sandia.gov/>, 2017.
2. D.L. Siebers, SAE Transactions 107 (3) (1998) 1205-1227.
3. L.M. Pickett, C.L. Genzale, J. Manin, Atom. Sprays 25 (5) (2015) 425-452.
4. SAE Standard J2715. Gasoline fuel injector spray measurement and characterization. Society of Automotive Engineers (2007).
5. P. Sphicas, L.M. Pickett, S. Skeen, J. Frank, T. Lucchini, D. Sinoir, G. D'Errico, K. Saha, S. Som, SAE Int. J. Fuels Lubr. 10 (1) (2017) 184-201.
6. F.R. Westlye, K. Penney, A. Ivarsson, L.M. Pickett, J. Manin, and S.A. Skeen, Appl.Opt. 56 (17) (2017) 5028-5038.
7. L.M. Pickett, C.L. Genzale, G. Bruneaux, L.-M. Malbec, L. Hermant, C.A. Christiansen, and J. Schramm, SAE Int.J.Engines 3 (2) (2010) 156-181.
8. M.P.B. Musculus, L.M. Pickett, Combust. Flame 141 (4) (2005) 371-391.
9. L.M. Pickett, J. Manin, C.L. Genzale, D.L. Siebers, M.P.B. Musculus, and C.A. Idicheria. SAE Int. J. Engines, 4(1) (2011) 764–799.
10. C. Crua, J. Manin, L.M. Pickett, Fuel 208 (2017):535-548.
11. R.N. Dahms, Phys.Fluids 28 (4) (2016) 042108.
12. F.R. Westlye, M. Battistoni, S.A. Skeen, J. Manin, L.M. Pickett, and A. Ivarsson. SAE 2016-01-0860 (2016).
13. L.M. Pickett, J. Manin, C.L. Genzale, D.L. Siebers, M.P.B. Musculus, C.A. Idicheria, SAE Int. J. Engines 4(1) (2011) 764-799.
14. M.P.B. Musculus, K. Kattke, SAE Int. J. Engines 2 (2009) 1170-1193.
15. R. Payri, J.P. Viera, H. Wang, L.-M. Malbec, Int. J. Multiphase Flow 80 (Supplement C) (2016) 69-78.
16. W.E. Eagle, M.P.B. Musculus, L.-M. Malbec, G.Bruneaux, Atom. Sprays 27 (6) (2017) 531-557.
17. J. Manin, L.M. Pickett, S.A. Skeen, J.H. Frank, COMODIA 2017.
18. S.A. Skeen, J. Manin, L.M. Pickett, Proc. Combust. Inst. 35 (3) (2015) 3167-3174.
19. R.N. Dahms, G.A. Paczko, S.A. Skeen, L.M. Pickett, Proc. Combust. Inst. 36 (2) (2017) 2615-2623.
20. J. Manin, L.M. Pickett, S.A. Skeen, SAE Int. J. Engines 6(4) (2013) 1908-1921.